First non-destructive internal imaging of *Rangea*, an icon of complex Ediacaran life

Alana C. Sharp[a,b,*], Alistair R. Evans[c,d], Siobhan A. Wilson[b], Patricia Vickers-Rich[b,e,f]

[a]School of Science and Technology, University of New England, NSW 2351, Australia

[b]School of Earth, Atmosphere and Environment, Monash University, Clayton, VIC 3800, Australia

[c]School of Biological Sciences, Monash University, Clayton VIC 3800, Australia

[d]Geosciences, Museums Victoria, Melbourne VIC 3001, Australia

[e]Faculty of Science, Engineering and Technology, Swinburne University, VIC Australia

[f]School of Life and Environmental Sciences, Deakin University, Burwood VIC Australia

* Corresponding author. Email: alana.c.sharp@gmail.com

Keywords: Ediacaran, Precambrian, computed tomography, *Rangea*, Aar Member, Namibia

Abstract

The origins of multicellular life have remained enigmatic due to the paucity of high-quality, three-dimensionally preserved fossils. *Rangea* was a centimetre- to decimetre-scale frond characterised by a repetitive pattern of self-similar branches and a sessile benthic lifestyle. Fossils are typically preserved as moulds and casts exposing only a leafy petalodium, and the rarity and incompleteness of specimens has made it difficult to reconstruct the three-dimensional (3D) morphology of the entire organism. This, in turn, has led to many differing interpretations of its morphology and phylogenetic affinities. Here we use high resolution X-ray micro-computed tomography (microCT) to investigate the 3D internal morphology of rare, exceptionally preserved ironstone fossils of *Rangea* from the Nama Group in southern Namibia. Our investigation reveals a series of structures that represent boundaries between individual fronds or structural elements that divide into smaller secondary and tertiary elements, leading to a repetitive pattern of branches. These elements surround an internal core of a distinctly different texture and internal appearance. There is no distortion of the walls of the primary elements, thus we conclude that *Rangea* likely had a rigid or semi-rigid skeleton-like structure that prevented buckling or compression and maintained integrity during life. We compare these findings with previous interpretations of *Rangea* morphology and present new insights on the architecture of internal structures, such as the central core, and the overall appearance of this complex Ediacaran life form. Our insights based on microCT scans of these rare, uniquely-preserved specimens provide a more accurate interpretation of the 3D morphology essential for determining the true affinities and modes of life of the Ediacaran biota during this early stage in the evolution of complex macroscopic life.

1. Introduction

Rangea was the first complex Precambrian macrofossil named and described anywhere in the world, and to this day is an iconic representative of Ediacaran biota (580–541 million years ago) (Gürich, 1933; Hoyal Cuthill and Conway Morris, 2014; Narbonne, 2004; Richter, 1955). Early interpretations of the morphology of *Rangea*, the type genus of rangeomorphs, regarded it as a primitive representative of living radial phyla, either Ctenophora (Gürich, 1929; Gürich, 1933) or Cnidaria (Richter, 1955). Most modern interpretations regard *Rangea*, and other rangeomorphs, as members of an extinct clade of the oldest large and complex organisms in Earth history (Brasier and Antcliffe, 2004; Erwin et al., 2011; Gehling and Narbonne, 2007; Narbonne, 2004; Seilacher, 1992, 2007; Xiao and Laflamme, 2009). The most common reconstructions of rangeomorph morphology are as fronds, elevated above the sea floor by a stalk attached to a holdfast or alternatively lying flat on the seabed, as in Newfoundland (Narbonne, 2004). However, a wide range of morphologies are preserved, including long-stemmed rangeomorph fronds with overlapping frondlets, short-stemmed fronds with pendant frondlets that hang from a thin central stalk, bush-shaped and spindle-shaped forms, and rangeomorphs with a quilted array of major and minor branches that overlay an internal organic skeleton (Narbonne, 2004).

Specimens of *Rangea* are rare and sometimes quite fragile, making it difficult to determine its three-dimensional morphology. This has led to many different interpretations. *Rangea* is normally reconstructed as a multifoliate, epibenthic frond consisting of several ‘vanes’ or ‘petaloids’ with a repetitive pattern of self-similar branches (Brasier et al., 2012; Jenkins, 1985; Laflamme and Narbonne, 2008a, b; Laflamme et al., 2009; Richter, 1955). These vanes are reconstructed as joining length-wise along their inner edge and radiate outwards from a central axis. Estimates of the number of vanes, or elements, in the *Rangea* petalodium have ranged from two to six (Dzik, 2002; Grazhdankin and Seilacher, 2005; Gürich, 1933; Jenkins, 1985; Pflüg, 1972; Richter, 1955; Vickers-Rich et al., 2013). Several

authors challenge this generally accepted view of *Rangea* morphology. Based on their horizontal orientation in preserving beds, Grazhdankin and Seilacher (2005) argued that *Rangea* must have been infaunal rather than an epibenthic frondose (Jenkins, 1985) or ovoid (Dzik, 2002) organism. Such orientation, however, as noted by Ivantsov et al. (2013), is simply an artefact of current flow during deposition of transported material. Grazhdankin and Seilacher (2005) described each element as a frond with a foliate shape consisting of a series of chevron-like units called 'quilts'. They also described a double-layered structure of the frond consisting of two membranes with the space between these membranes inflated and fractally quilted. Dzik (2002) described *Rangea* as tetraradially symmetrical with a possible sand-filled rachis and bulb, and argued for *Rangea*'s affinity with ctenophores. Dzik (2002) also argued that the fossilisation process did not reproduce the original external morphology but rather the inner surface of collapsed organs, describing *Rangea* as having complex internal anatomy, a smooth external surface of the body and radial membranes.

Recently, Ediacaran fossils recovered from Farm Aar in southern Namibia have greatly increased the number of known *Rangea* fossils with more than 100 specimens discovered (Vickers-Rich et al., 2013). The majority of these were recovered from small storm-induced channel deposits and preserved in siliciclastic rocks. Many exhibit three-dimensional preservation, which has revealed previously unrecorded morphology (Vickers-Rich et al., 2013) that supports a six-fold symmetry, at least in this assemblage. The two specimens reported on here are extremely rare and uniquely preserved as ironstone petrifactions (Fig. 1a). These were found on a deflation surface near the base of the late Neoproterozoic Aar Member of the Dabis Formation, Nama Group, and are likely fragments of one individual organism.

This unique form of three-dimensional preservation as ironstone allowed us to examine the structure of *Rangea* in more detail using non-destructive methods such as X-ray

microcomputed tomography (microCT). Here we use microCT to compare these specimens with previous interpretations of *Rangea* morphology to clarify the number and arrangement of fronds, and the presence or absence of a cone-shaped central core and external tubes as presented in the description in Vickers-Rich et al. (2013). Our interpretation of *Rangea* morphology supports the classic interpretations of frond morphology in some instances, and in turn raises further questions, yet unresolved.

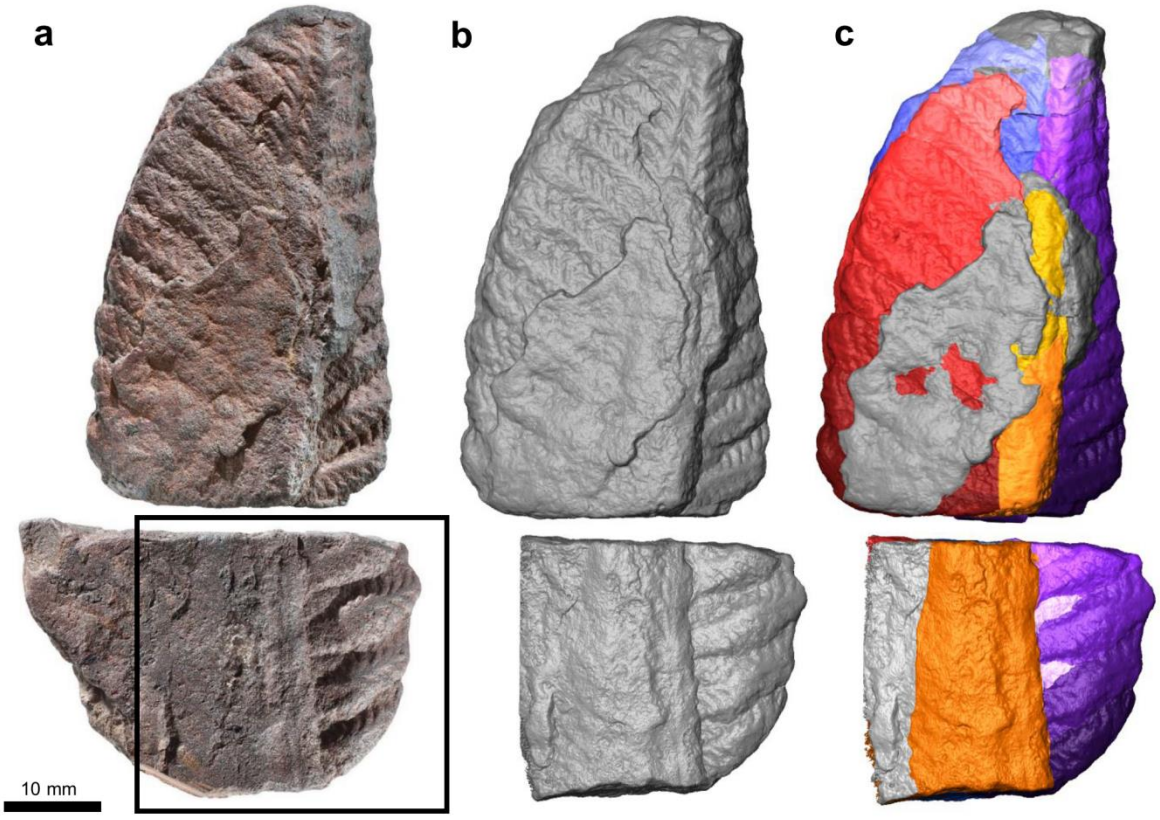

Fig. 1. Unique ironstone preservation of *Rangea* fossils shows fine details of frond elements and internal structures. (A) Photographs of the two specimens of *Rangea* with NESMF649 (top) and NESMF650 (bottom). The box represents the area scanned in specimen NESMF650. (B) Surface rendered 3D models showing the pattern produced by the second- and third-order elements. Note the lack of distortion of these elements. (C) Segmented volume model of *Rangea* showing each primary element (red, blue, purple) with different shades of colour

representing the secondary elements, and the axial core (orange and yellow). Grey areas are matrix or areas that could not be assigned to one of the three primary elements or axial core.

2. Methods

2.1. Specimens

Fossils were recovered from surface exposures under permit from the National Heritage Council of Namibia (Permit number 6 of 2011, to P.V-R.). Specimens are deposited with the Geological Survey of Namibia, National Earth Science Museum (NESM) in Windhoek. Two of these specimens, NESM F649 and NESMF650 (Fig. 1a), are reported on here.

2.2. Thin sectioning

A thin section of NESMF650 was produced to obtain textual and compositional information about the mineralogy, and thus the mode of preservation, of this specimen. The section was trimmed to size with a diamond saw, and the glass "face" was lapped flat on diamond laps and hand lapped on glass with 10 micron aluminium oxide. The sample was dried and vacuum impregnated with 2 part epoxy, allowed to dry and lapped flat again. Using the same epoxy, the sample was glued to the slide, and excess sample cut off with a Diam saw and machine lapped down to a thickness of approximately 40 µm. The sample was then hand lapped to 30 µm and a coverslip attached with UV resin.

2.3. Scanning Electron Microscopy

Back Scattered Electron (BSE) images and Energy Dispersive X-ray Spectra (EDS) were collected from the carbon-coated polished thin section of NESMF650 using a JEOL 7001F FEG-SEM at the Monash Centre for Electron Microscopy. The microscope was operated at an accelerating voltage of 15 kV with a working distance of 10 mm.

2.4. Powder X-ray Diffraction

Powder X-ray diffraction (XRD) data were collected to better understand the mineralogy, and thus the taphonomy, of the *Rangea* specimens. A small subsample of the fossil specimen NESMF650 was removed with a Dremel tool and pulverised by hand under ethanol using an agate mortar and pestle. The subsample was mounted as an ethanol slurry onto a zero-background quartz plate for collection of powder XRD data. An XRD pattern was collected at the Monash X-ray Platform using a Bruker D8 Advance Eco X-ray Diffractometer. The pattern was obtained using a Cu X-ray tube (operated at 40 kV and 25 mA) over the range from 3–70° 2θ using a step size of 0.02° 2θ and a dwell time of 2.8 s/step.

Mineral phases were identified with reference to the Powder Diffraction File 2 (PDF-2) database available from the International Center for Diffraction Data (ICDD) using the DIFFRAC^{plus} EVA v.4 software program (Bruker AXS). An estimate of phase abundances was obtained by Rietveld refinement (Bish and Howard, 1988; Hill and Howard, 1987; Rietveld, 1969) using the program Topas v.4.2 (Bruker AXS). This estimate is semi-quantitative owing to data collection from a thin film of hand-pulverised material on a zero-background quartz plate.

2.5. X-ray micro-computed tomography

Specimens NESM F649 and NESMF650 (Fig 1a) were scanned separately at the Monash University X-ray Microscope Facility for Imaging Geomaterials (XMFIG) using an Xradia XRM Versa 520 microCT scanner at 160 kV and 62 µA for 1601 projections at 3 s exposure, resulting in 35 µm isometric voxels. NESMF649 was scanned in two parts owing to its larger size. The data were converted to 8 bit TIFF image stacks (2×1004 for NESMF649 and 1004 for NESMF650) and imported into Avizo 9.0 for visualisation and segmentation.

The internal detail of each specimen was visualised as orthoslices and the volumes were segmented into individual components using manual selection tools. The clarity of divisions between elements was more visible in some axes than others, so segmentation was performed in all three axes using a systematic approach; the structures were first selected in the transverse axis and later edited in the remaining axes where other structures were more visible. Each major element was assigned a different colour (red, blue or purple), and divisions within these elements were graded from light to dark. A 3D surface was produced for each element for easy visualisation. Our use of these methodologies and analytical techniques maximised recovery of the morphological details of these uniquely preserved specimens. The microCT data will be made available at Figshare.com.

3. Results

3.1. Mineralogical Composition

Rangea specimens are commonly preserved by jarosite [$(K,Na,H_3O)Fe_3(SO_4)_2(OH)_6$] as moulds or casts that show only a leafy petalodium (e.g., Vickers-Rich et al., 2013). The mineralogical composition of the smaller specimen in this study (NESMF650) is dominated by quartz (76.7 wt.%; see Fig. S1 for the Rietveld refinement plot). Less abundant phases are

hematite (20.9 wt.%), goethite (1.7 wt.%), muscovite (0.5 wt.%) and Mg-calcite (0.2 wt.%). The size of quartz grains is larger within the axial core (Fig. 2a), but all grains exhibit high intragranular porosity visible using scanning electron microscopy (Fig. 2a–d). Hematite and goethite occur as micrometre-scale rosettes of platy crystals within the intergranular spaces in the specimen (Fig. 2b). Altered detrital muscovite occurs in the intergranular spaces between quartz crystals and it is commonly intermixed with platelets of hematite (Fig. 2c and d) to form anastomosing veins that fill the pore network. Muscovite grains within these veins are consistently split along the basal cleavage where hematite has grown. The low abundance of Mg-calcite is likely a component of intergranular cement.

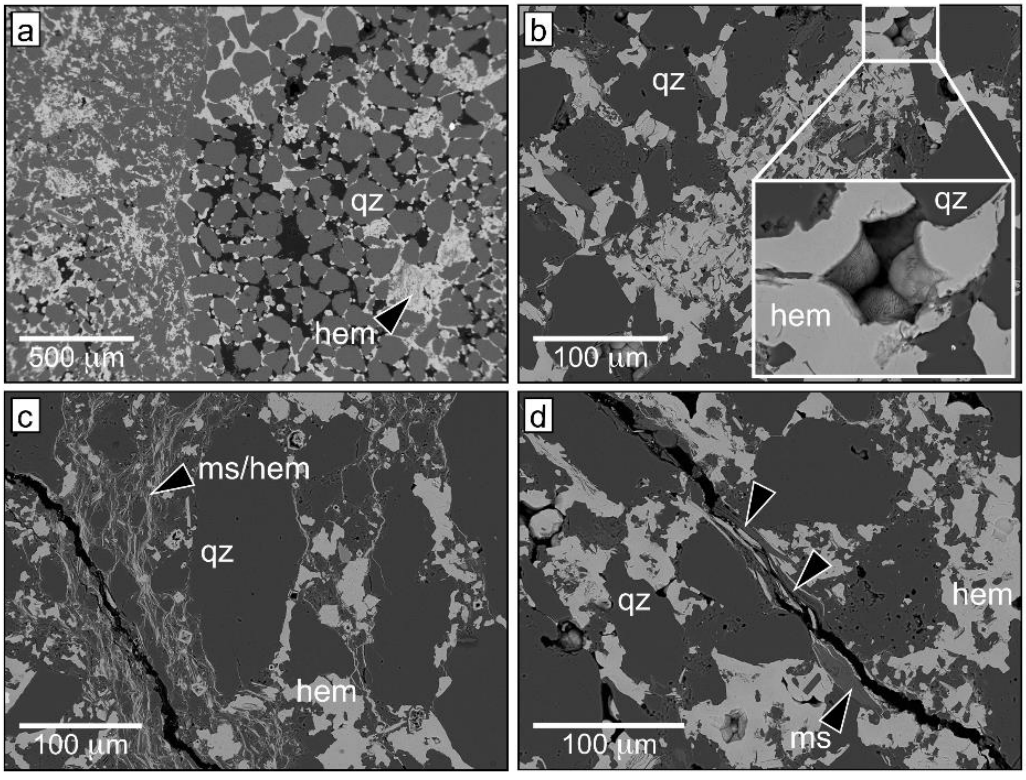

Fig. 2. Backscattered electron micrographs of a thin section through sample NESMF650. (A) Detrital grains of quartz (qz) at the interface between the axial core (at the right half of the image) and an adjoining primary element. There is notably more intergranular porosity in the fossilised core than in the surrounding primary elements. Rosettes of hematite can be seen infilling this pore space, which is mostly consumed by hematite in the left half of the image

(within the primary element). (B) Some parts of the specimen have been heavily altered during dissolution–precipitation of quartz and hematite, giving rise to complex textures. The inset in B shows detail of hematite rosettes, which are composed of fine platelets of this mineral. (C, D) Intermixed muscovite and micrometre-scale platelets of hematite form anastomosing veins around quartz grains. The arrows in D point to relatively unaltered veins of muscovite, sheets of which are commonly split along the basal cleavage where hematite has grown. Intragranular porosity in quartz crystals is high and grain boundaries are irregular, features that are consistent with dissolution–precipitation of quartz during diagenesis.

3.2. MicroCT Analysis

MicroCT images (Fig. 3, Fig. S2-S5, and Supplementary Videos 1 and 2) reveal the arrangement of fronds, or elements, within the fossil and show three orders of self-similar branching, or divisions of complexity, plus the internal features of an axial core. Three elements (of the hypothesised six) are connected to the core along its longitudinal extent (presented here in Fig. 1c in three different colours). In cross-sections of the larger specimen (NESMF649), two of these primary elements (red and blue) have been compressed in the transverse plane, red more so than blue, whereas the third element (purple) appears relatively uncompressed (Fig. 3e). There does not appear to be any compression along the longitudinal axis of the specimen, suggesting a structural rigidity that prevented distortion during life and even during preservation.

The three primary elements are divided into a second order of complexity, presented as shades from light to dark within each of the primary elements (Fig. 1c). These secondary elements radiate upwards at an angle of approximately 60 degrees from the longitudinal axis of the central core, producing a series of stacked sections within each primary element. The secondary elements gradually decrease in height from the base of the specimen towards its apex. The boundary between each of the primary elements is characterised by an oscillating,

212 zig-zag pattern produced by the offset nature of secondary elements – one set of secondary
213 elements is offset by one half the length of the secondary elements in the neighbouring primary
214 element (Fig. 3a). The third order of complexity is visible within the secondary elements as
215 small, tertiary branches radiating from the midline of each secondary element (Fig. 1). The
216 architecture of these tertiary elements is visible only on the external face of the specimen;
217 however, we hypothesise that this pattern was replicated on both sides of the primary elements
218 (between red and blue, and blue and purple) during life, as supported by the preservation of the
219 structure of the second-order elements.

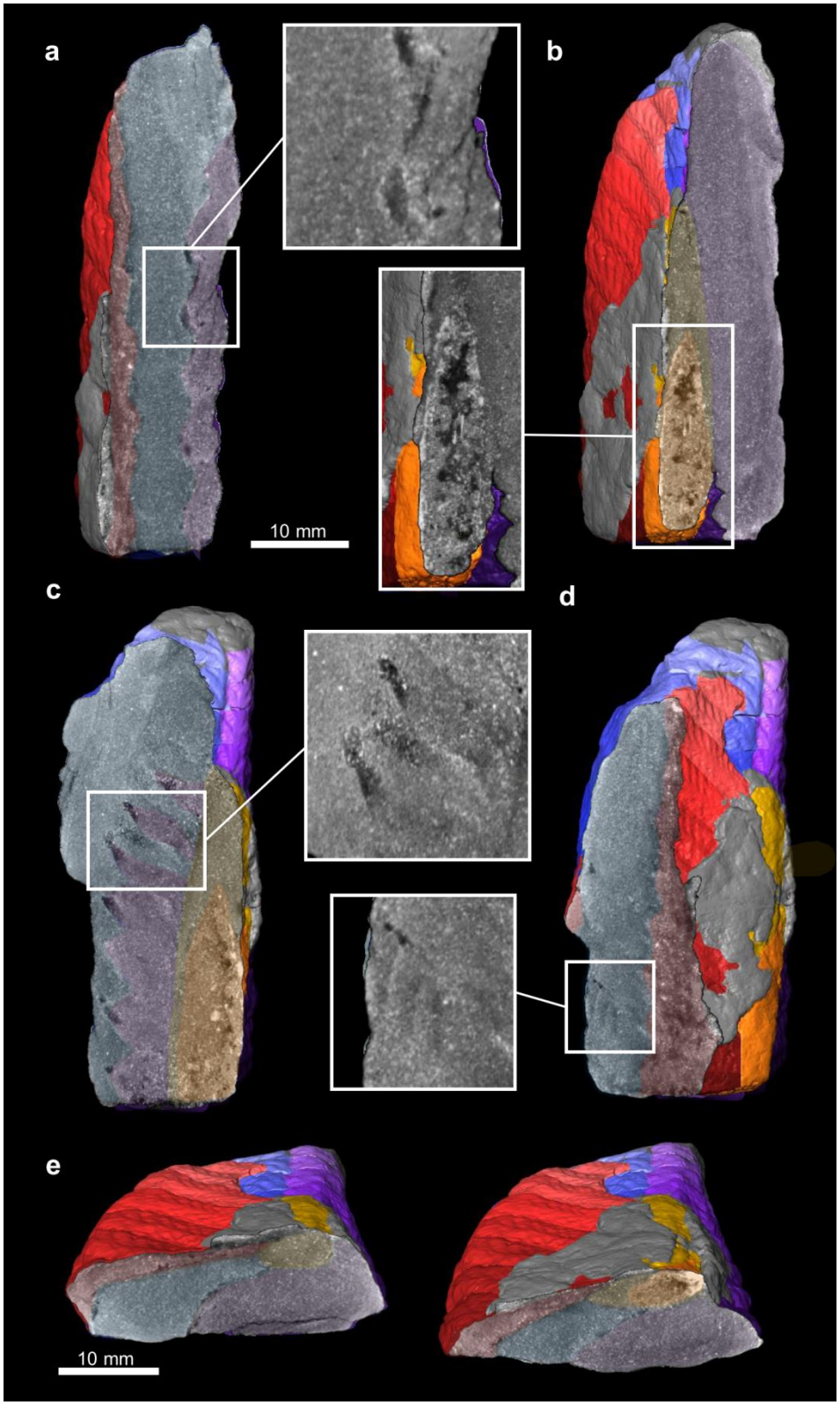

Fig. 3. Detailed internal structures of *Rangea* NESMF649 revealed by microCT imaging. (A) Zig-zag boundary between primary elements produced by the offset nature of the secondary elements; (B) internal cone-shaped axial core; (C) internal boundary between the blue and purple primary elements to the left of the axial core; (D) detail of tertiary element structure;

(E) cross sections showing relative compression of the frond elements. Transparent colour overlays have been added to show the regions of each structure; see Fig. S2 for uncoloured versions.

The internal structure revealed by microCT was confirmed during analysis of the thin section through NESMF650, including the presence of boundaries between elements and the internal axial core. Spatial variation in mineralogical composition of the specimen (Fig. 4a) corresponds to differences in electron density revealed by the X-ray microCT (Fig. 4b).

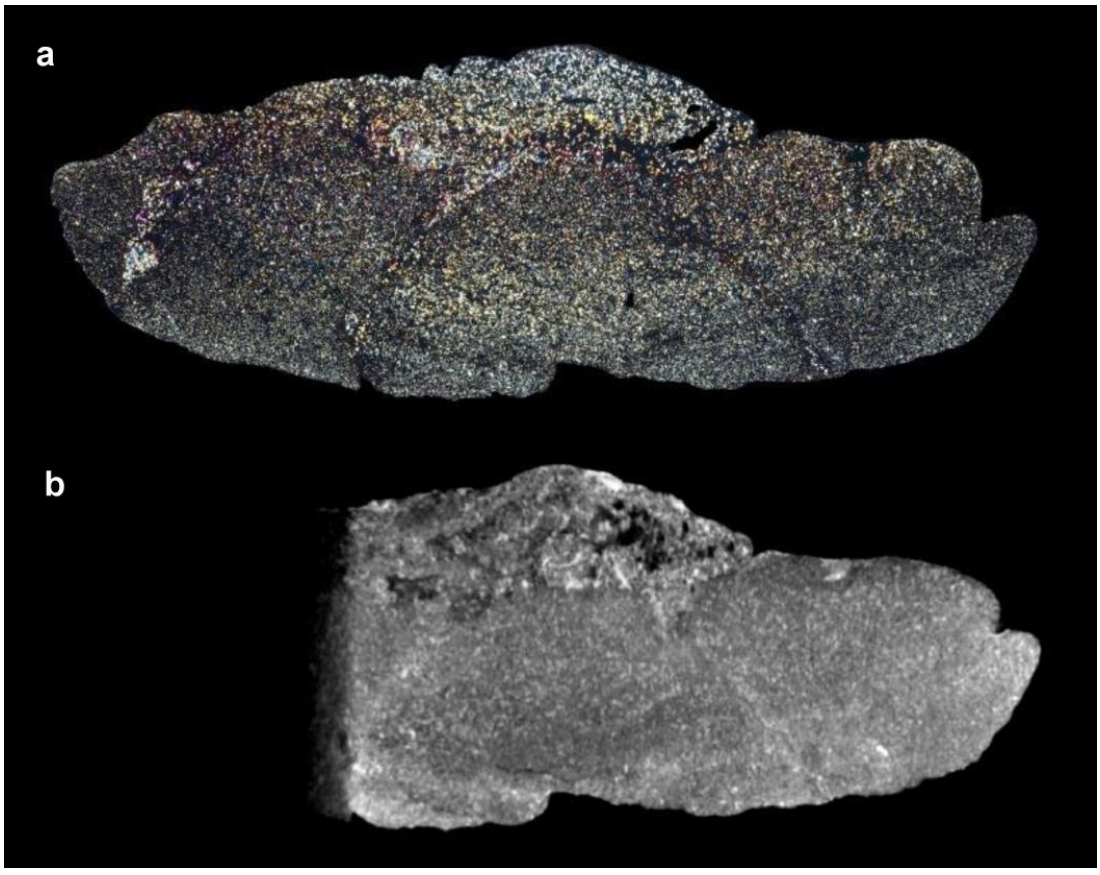

Fig. 4. Confirmation of internal structure of *Rangea* NESMF650 through microCT, and thin section. (A) Thin section photographed under cross-polar light. (B) Equivalent section in microCT volume.

4. Discussion

4.1. Mechanism of preservation

The soft-bodied Ediacaran biota are typically preserved as moulds or cast in sandstones, and are rarely preserved with the 3D morphology of the entire organism intact. Ediacaran-style preservation is thought to have been aided by microbial mats that covered the sea floor, producing Fe-sulfide "death masks" of the external morphology (Gehling, 1999; Laflamme et al., 2011). These death masks were produced by heterotrophic sulfate-reducing bacteria that mediated precipitation of Fe-sulfide minerals during decomposition of the organic matter of the organism. This would have produced a mineralised layer around the outside of the organism. This mode of preservation, however, does not provide detail of the internal morphology of the organism, which we see in these ironstone specimens. The high abundance of quartz found within these specimens is consistent with infilling of the organism by detrital quartz in a marine environment and preservation in sandstone. Some of this quartz may have been associated with precipitation of a silica cement (Tarhan et al., 2016), but the presence of discrete grains as well as the high intragranular porosity suggests dissolution–precipitation of detrital quartz (Putnis, 2015), possibly via pressure solution originating at quartz–mica grain boundaries post-burial as observed by Oelkers et al., (1996). This analysis cannot be used to identify multiple generations of quartz; however, cathodoluminescence microscopy could be employd to distinguish between primary detrital quartz and recrystallised quartz cements (e.g., Oelkers et al., 1996).

Hematite, the second most abundant mineral phase in the specimen, is a common dehydration product of goethite in sediments and gives the sample its dark maroon colour. Goethite, which is present at low abundance in the specimen, commonly forms under circumneutral to alkaline pH conditions via precursor phases including jarosite,

schwertmannite, or ferrihydrite, which are oxidative weathering products of iron sulfides such as pyrite (Davidson et al., 2008; Zolotov and Shock, 2005; Schieber, 2011; Schweitzer et al., 2013). The high abundance of Fe-oxyhydroxide minerals in the sample implies interaction with an iron-bearing fluid during diagenesis. The source of this iron could have been oxidation of sulfide precursor minerals, which have been shown to play a role in preservation of *Rangea* previously (Vickers-Rich et al., 2013), or alteration of Fe-rich clay minerals or micas under acidic and oxidising conditions (Webb et al., 2003). The combination of infilling of the internal structures by detrital quartz and diagenetic cementation by silica and hematite may have played a role in the exceptional preservation of these fossils. Infilling by detrital quartz would have afforded a rigidity to the structure while still providing sufficient pore space for formation of hydrated Fe-bearing alteration phases without inducing deformation via reaction-driven cracking.

4.2. Morphological interpretation

There have been numerous interpretations of the morphology of *Rangea* from an epibenthic frondose (Jenkins, 1985) or ovoid (Dzik, 2002) organism, to an infaunal rather than epibenthic organism (Grazhdankin and Seilacher, 2005), and with the number of vanes, or elements, ranging from two to six (Dzik, 2002; Grazhdankin and Seilacher, 2005; Gürich, 1933; Jenkins, 1985; Pflüg, 1972; Richter, 1955; Vickers-Rich et al., 2013). The uniquely preserved ironstone specimens of *Rangea* described here allowed us to examine the morphology using 3D microCT which revealed the internal arrangement of structures, including a cone-shaped axial core. The interpretation presented here in part supports, and in part challenges, previous reconstructions of *Rangea* as having a more inflated, bulb-like morphology of six elements surrounding a central core, rather than thin lobes or sheets (Gehling, 1999). The model provided in Vickers-

Rich et al. (2013), with the removal of the tubes at the end of the petaloids and a marked inflation of the primary elements would perhaps provide a description of what we have observed in these ironstone specimens.

Grazhdankin and Seilacher (2005) described the primary "quilts" (a series of chevron-like units; analogous to the secondary elements here) of each frond as having two rows – long primary quilts and short subsidiary quilts. They suggested that these subsidiary quilts terminated a short distance from the central axis and the primary quilts continued to the edge of the frond. The presence of these subsidiary structures was also noted by Vickers-Rich et al. (2013); however, they did not speculate on the terminal morphology of the subsidiary quilts. Here, we are able to identify the subsidiary branches and describe their 3D structure (Fig 1c). These structures do indeed taper out a short distance from the axis core (~7 mm) without reaching the length of the primary quilts. There is no evidence for a marginal tube running along the length of each vane distally as reconstructed in Vickers-Rich et al. (2013). Instead, the rounded ends of each secondary branch on one side (as observed on the red element) are closely stacked along the external longitudinal axis.

Dzik (2002) suggested that the fossilisation process did not reproduce the original external morphology but rather the inner surface of collapsed organs, describing *Rangea* as having complex internal anatomy, a smooth external surface, and radial membranes. We partly agree with this interpretation; however, we disagree that these structures are analogous to organs. We interpret the boundary between the primary, secondary and tertiary elemental structures preserved on our *Rangea* specimens as a semi-rigid supporting layer, or structures, for the internal tissues of the organism. In the scans, these structures separate the primary elements like sheets that appear to be tightly compressed together.

We put forward two hypotheses for this observation. In the first hypothesis, the primary elements may have been tightly connected during life, with the sheet-like supporting structures separating the elements at the primary, secondary and tertiary level. For this hypothesis, an external membrane or sheath would encase the entire organism producing a smooth external appearance in agreement with Dzik (2002). Based on this hypothesis, the specimens we have studied would have had six primary elements, three of which have not been preserved, and the smooth side of the specimens would in fact be the external face of the organism. The outer membrane would have provided flexibility to the structure and allowed the elements to compress during fossilisation (as observed in the red and blue elements), while the rigid sheets prevent compression in the longitudinal axis.

Alternatively, the primary elements may have been separate from one another in life, and compressed together during fossilisation, with the semi-rigid structures surrounding the internal content at the primary, secondary and tertiary levels like an infolded sheet. In this interpretation there would be no membrane or sheath surrounding the organism but rather a semi-rigid casing surrounding each element. This hypothesis is also supported by the observation that one element (the red element) has more tertiary elements preserved than the other externally visible element (the purple element). This suggests that the purple element was damaged or torn and potentially filled with external fluid during fossilisation.

The nature of the base of *Rangea* has remained largely unknown and quite controversial owing to typically poor preservation as moulds that only reveal a leafy petalodium. The discovery and subsequent description of the base and axial core of *Rangea* was illustrated in the recent reconstruction by Vickers-Rich et al. (2013) as a hexaradial, bulb-like structure running up the centre of the organism, and tapering to the tip like a cone. Our microCT scans confirm this observation that the axial core has a cone-shaped internal region with a tapered tip

dorsally (Fig. 3b) and a superior portion that has a convex end toward the apex of the specimen. The internal cone is distinguished by an obvious difference in tone (which reflects electron density contrast in microCT data) and grain size from the superior portion of the core, and the surrounding structures (elements), representing a different mineralogical composition to the rest of the specimen. In order to remain rigid, un-collapsible and upright in the water column, the lower part may have been sediment-filled, as suggested by Dzik (2002), and the upper part may have been liquid or gel-filled as with the surrounding elements. The nature of the base cannot be determined based on the two ironstone specimens available because this region was not preserved.

In conclusion, the 3D interpretation of *Rangea* morphology presented here in part supports and in part challenges aspects of previous reconstructions. Rather than a series of relatively thin lobes or sheets of elements radiating out from a central stalk, we have identified structures that resemble thick wedges (the primary elements), which in preservation lie closely associated with their neighbours on either side. The structures bounding the elements were likely rigid, or semi-rigid, to provide stability and resistance to mechanical stress during life. The determination of the true affinities and modes of life of the Ediacaran biota relies on accurate interpretation of 3D morphology. Our findings represent a significant advance in this direction, and the application of our methods to similarly well-preserved material of other Ediacaran organisms will aid in resolving the mysteries of the earliest complex life.

Acknowledgments Sincere thanks to Barbara Bohem-Erni, Farm Aar, for her continued support for our work in southern Namibia, the Namibian Geological Survey (especially Gabi Schneider and Helke Moeke), the National Geographic Society (Grant 9208-12 to P. V-R.) and the International Geosciences Program and the Australian Committee of UNESCO IGCP for

our projects IGCP493 and 587 for funding. We thank Robert Smith and Mary Gilroy of Federation University for the thin section, Andy Tomkins and Alastair Tait of Monash University for advice on mineral textures, Steven Morton for photography and Peter Trusler for constructive feedback throughout. We also thank two anonymous reviewers for their valued feedback and Professor Parrish for editorial handling of this manuscript.

References

Bish, D.L., Howard, S.A., 1988. Quantitative phase analysis using the Rietveld method. Journal of Applied Crystallography 21, 86-91.

Brasier, M., Antcliffe, J., 2004. Decoding the Ediacaran Enigma. Science 305, 1115.

Brasier, M.D., Antcliffe, J.B., Liu, A.G., 2012. The architecture of Ediacaran fronds. Palaeontology 55, 1105-1124.

Davidson, L.E., Shaw, S., Benning, L.G., 2008. The kinetics and mechanisms of schwertmannite transformation to goethite and hematite under alkaline conditions. American Mineralogist 93, 1326-1337.

Dzik, J., 2002. Possible ctenophoran affinities of the Precambrian "sea-pen" *Rangea*. Journal of Morphology 252, 315-334.

Erwin, D.H., Laflamme, M., Tweedt, S.M., Sperling, E.A., Pisani, D., Peterson, K.J., 2011. The Cambrian Conundrum: Early Divergence and Later Ecological Success in the Early History of Animals. Science 334, 1091.

Gehling, J.G., 1999. Microbial mats in terminal Proterozoic siliciclastics: Ediacaran death masks. Palaios 14, 40-57.

Gehling, J.G., Narbonne, G.M., 2007. Spindle-shaped Ediacara fossils from the Mistaken Point assemblage, Avalon Zone, Newfoundland. Canadian Journal of Earth Sciences 44, 367-387.

Grazhdankin, D., Seilacher, A., 2005. A re-examination of the Nama-type Vendian organism *Rangea schneiderhoehni*. Geological Magazine 142, 571-582.

Gürich, G., 1929. Die bislang ältesten Spuren von Organismen in Südafrika, International Geological Congress. South Africa, pp. 670-680.

Gürich, G., 1933. Die Kuibis-Fossilien der Nama-Formation von Südwestafrika. Palaeontologische Zeitschrift 15, 137-154.

Hill, R.J., Howard, C.J., 1987. Quantitative phase analysis from neutron powder diffraction data using the Rietveld Method. Journal of Applied Crystallography 20, 467-474.

Hoyal Cuthill, J.F., Conway Morris, S., 2014. Fractal branching organizations of Ediacaran rangeomorph fronds reveal a lost Proterozoic body plan. Proceedings of the National Academy of Sciences 111, 13122-13126.

Jenkins, R.J.F., 1985. The enigmatic Ediacaran (late Precambrian) genus *Rangea* and related forms. Paleobiology 11, 336-355.

Laflamme, M., Narbonne, G.M., 2008a. Competition in a Precambrian world: palaeoecology of Ediacaran fronds. Geology Today 24, 182-187.

Laflamme, M., Narbonne, G.M., 2008b. Ediacaran fronds. Palaeogeography, Palaeoclimatology, Palaeoecology 258, 162-179.

Laflamme, M., Xiao, S., Kowalewski, M., 2009. Osmotrophy in modular Ediacara organisms. Proceedings of the National Academy of Sciences 106, 14438-14443.

Laflamme, M., Schiffbauer, J.D., Narbonne, G.M., Briggs, D.E.G., 2011. Microbial biofilms and the preservation of the Ediacaran biota. Lethaia 44, 203-213.

Narbonne, G.M., 2004. Modular Construction of Early Ediacaran Complex Life Forms. Science 305, 1141-1144.

Oelkers, E.H., Bjørkum, P.A., Murphy, W.M., 1996. A petrographic and computational investigation of quartz cementation and porosity reduction in North Sea sandstones. American Journal of Science 296, 420-452.

Pflüg, H.-D., 1972. Systematik der jung-präkambrischen PetalonamaePflug 1970. Paläontol Z 46, 56-67.

Putnis, A., 2015. Transient porosity resulting from fluid-mineral interaction and its consequences. Reviews in Mineralogy & Geochemistry 80, 1-23.

Richter, R., 1955. Die altesten Fossilien Sd-Afrikas. Senckenbergiana lethaea 36, 24389.

Rietveld, H.M., 1969. A profile refinement method for nuclear and magnetic structures. Journal of Applied Crystallography 2, 65-71.

Schieber, J., 2011. Iron Sulfide Formation, in: Ritner, J., Thiel, V. (Eds.), Encyclopedia of Geobiology. Springer Verlag, pp. 486-502.

Schweitzer, M.H., Zheng, W., Cleland, T.P., Goodwin, M.B., Boatman, E., Theil, E., Marcus, M.A., Fakra, S.C., 2013. A role for iron and oxygen chemistry in preserving soft

tissues, cells and molecules from deep time. Proceedings of the Royal Society B: Biological Sciences 281.

Seilacher, A., 1992. Vendobionta and Psammocorallia: lost constructions of Precambrian evolution. Journal of the Geological Society 149, 607-613.

Seilacher, A., 2007. The nature of vendobionts. Geological Society, London, Special Publications 286, 387-397.

Tarhan, L.G., Hood, A.v.S., Droser, M.L., Gehling, J.G., Briggs, D.E.G., 2016. Exceptional preservation of soft-bodied Ediacara Biota promoted by silica-rich oceans. Geology.

Vickers-Rich, P., Ivantsov, A.Y., Trusler, P.W., Narbonne, G.M., Hall, M., Wilson, S.A., Greentree, C., Fedonkin, M.A., Elliott, D.A., Hoffmann, K.H., Schneider, G.I.C., 2013. Reconstructing *Rangea*: New Discoveries from the Ediacaran of Southern Namibia. Journal of Paleontology 87, 1-15.

Webb, A.D., Dickens, G.R., Oliver, N.H.S., 2003. From banded iron-formation to iron ore: geochemical and mineralogical contstraints from across the Hamersley Province, Western Australia. Chemical Geology 197, 215-251.

Xiao, S., Laflamme, M., 2009. On the eve of animal radiation: phylogeny, ecology and evolution of the Ediacara biota. Trends in Ecology & Evolution 24, 31-40.

Zolotov, M.Y., Shock, E.L., 2005. Formation of jarosite-bearing deposits through aqueous oxidation of pyrite at Meridiani Planum, Mars. Geophysical Research Letters 32, L21203.

Supplementary Figures

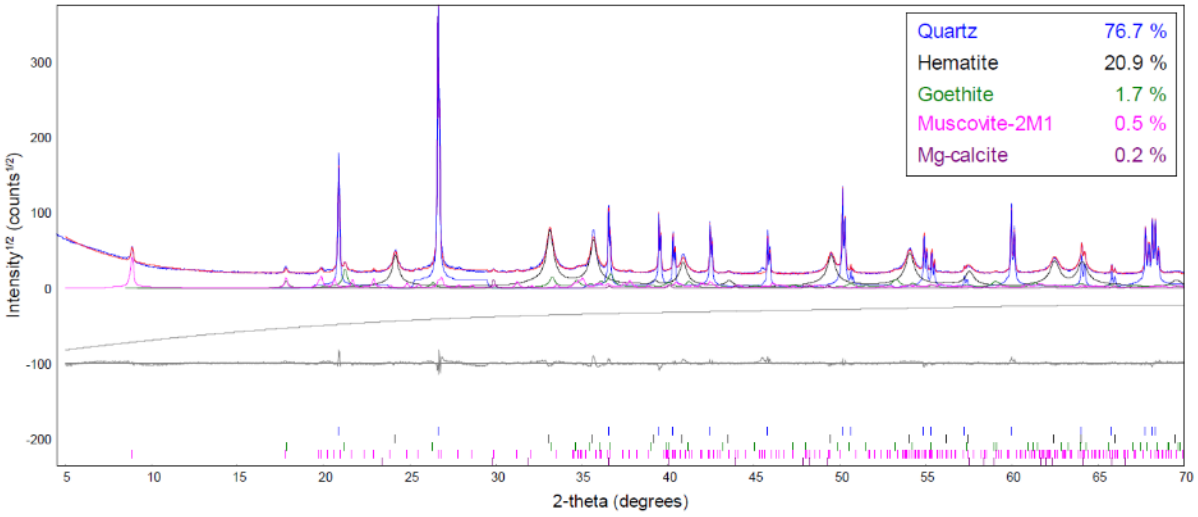

441

442 **Fig. S1.** Rietveld refinement results for sample NESMF650. Uppermost lines = observed data
443 (in black) overlain by calculated pattern (in red); curves under the observed and calculated
444 patterns = calculated patterns of each phase, colour coded by mineral. Grey curve below =
445 background function; lowermost black line = residual pattern showing misfit between data and
446 model; vertical lines = positions of Bragg reflections for each phase. Axes are intensity
447 (in square root counts) versus 2θ (degrees) for Cu Kα radiation. The weighted pattern index,
448 R_{wp}, for the refinement is 9.6%.

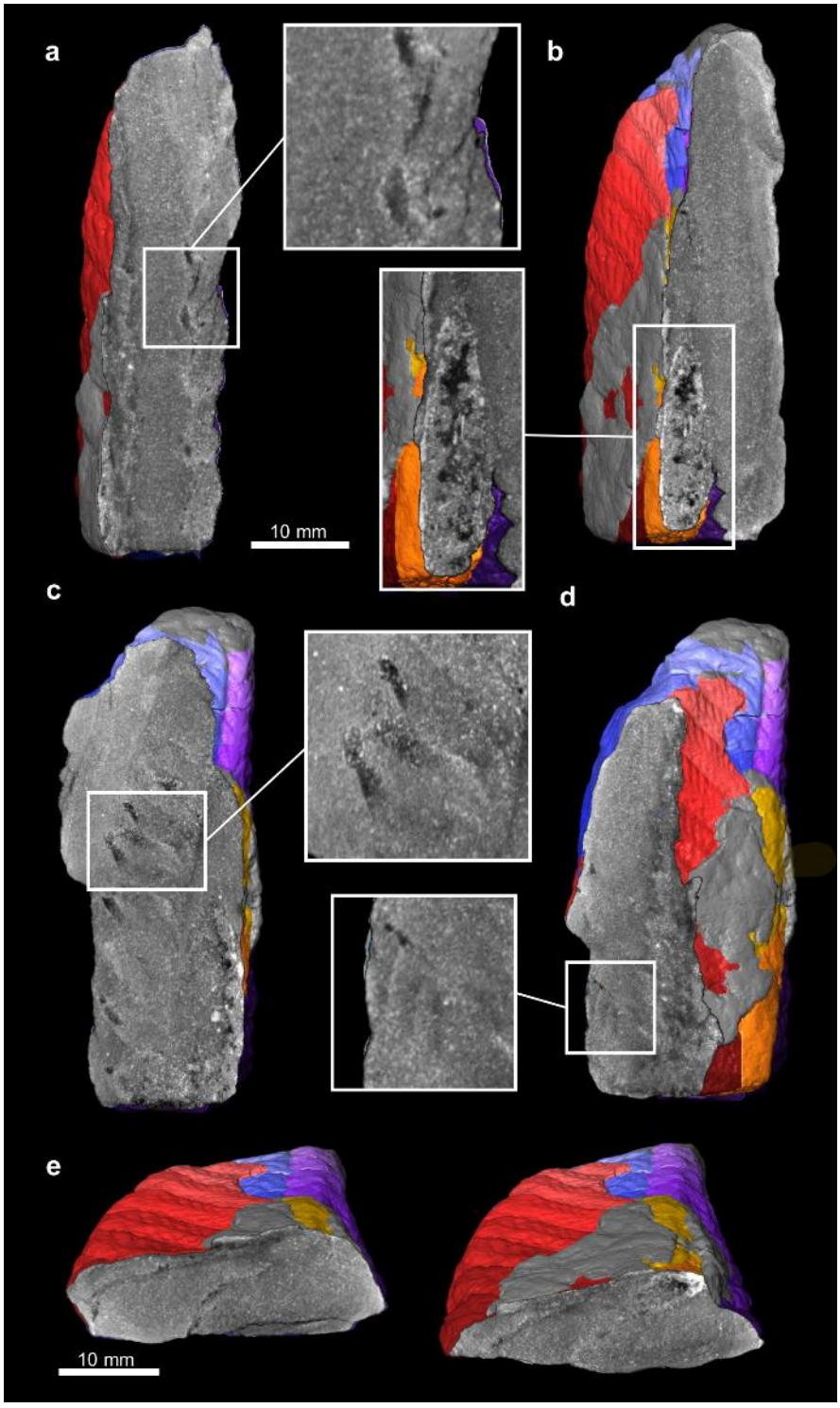

Fig. S2. Uncoloured CT sections though *Rangea* NESMF649 showing key internal structure. (A) zig-zag boundary between primary elements produced by the offset nature of the secondary elements; (B) internal cone-shaped axial core; (C) internal boundary between the blue and purple primary elements to the left of the axial core; (D) detail of tertiary element structure; (E) cross sections showing relative compression of the frond elements.

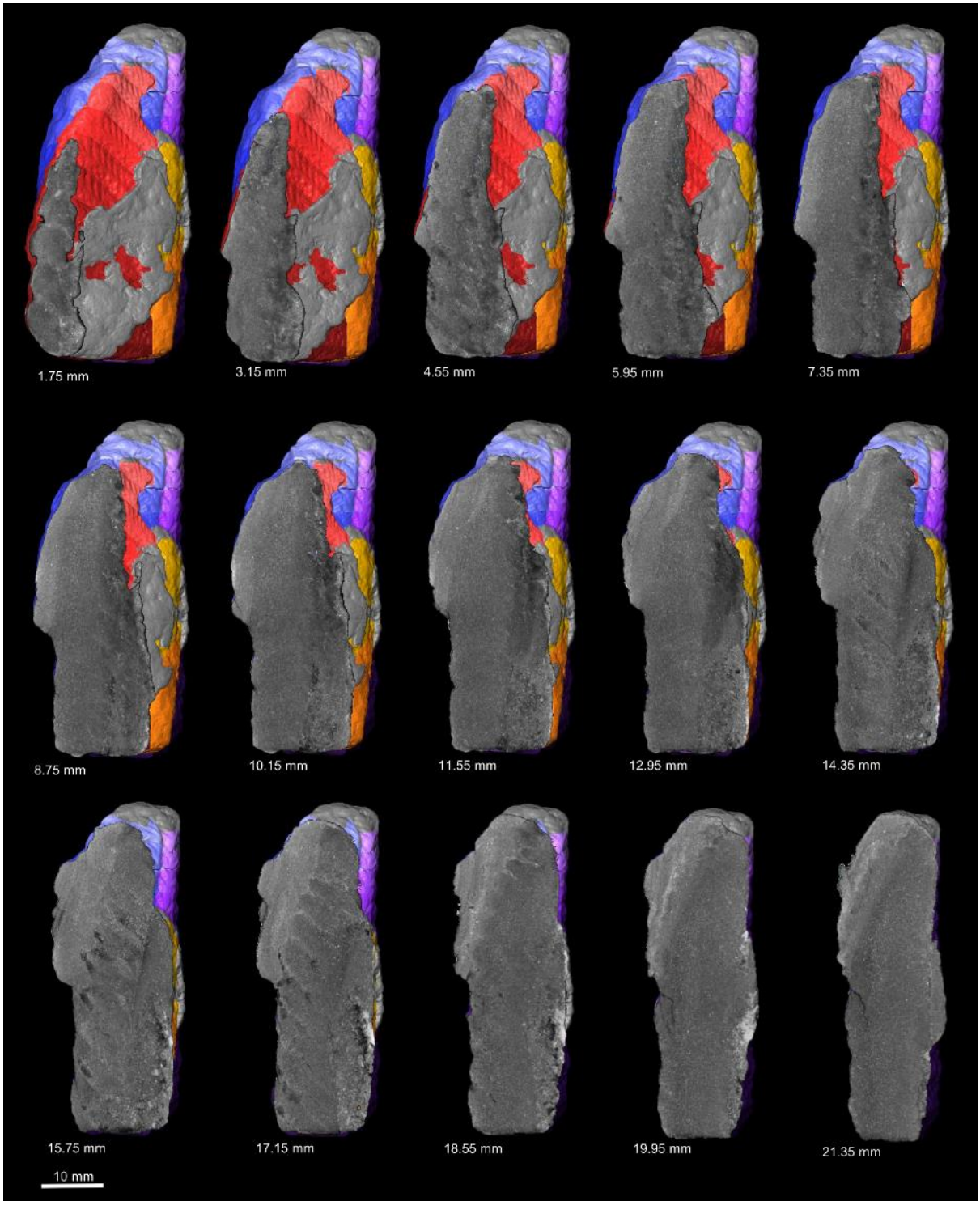

Fig. S3. CT sections though *Rangea* NESMF649 in the longitudinal axis. The location of each section (numbered) is 1.40 mm from the previous section in the series.

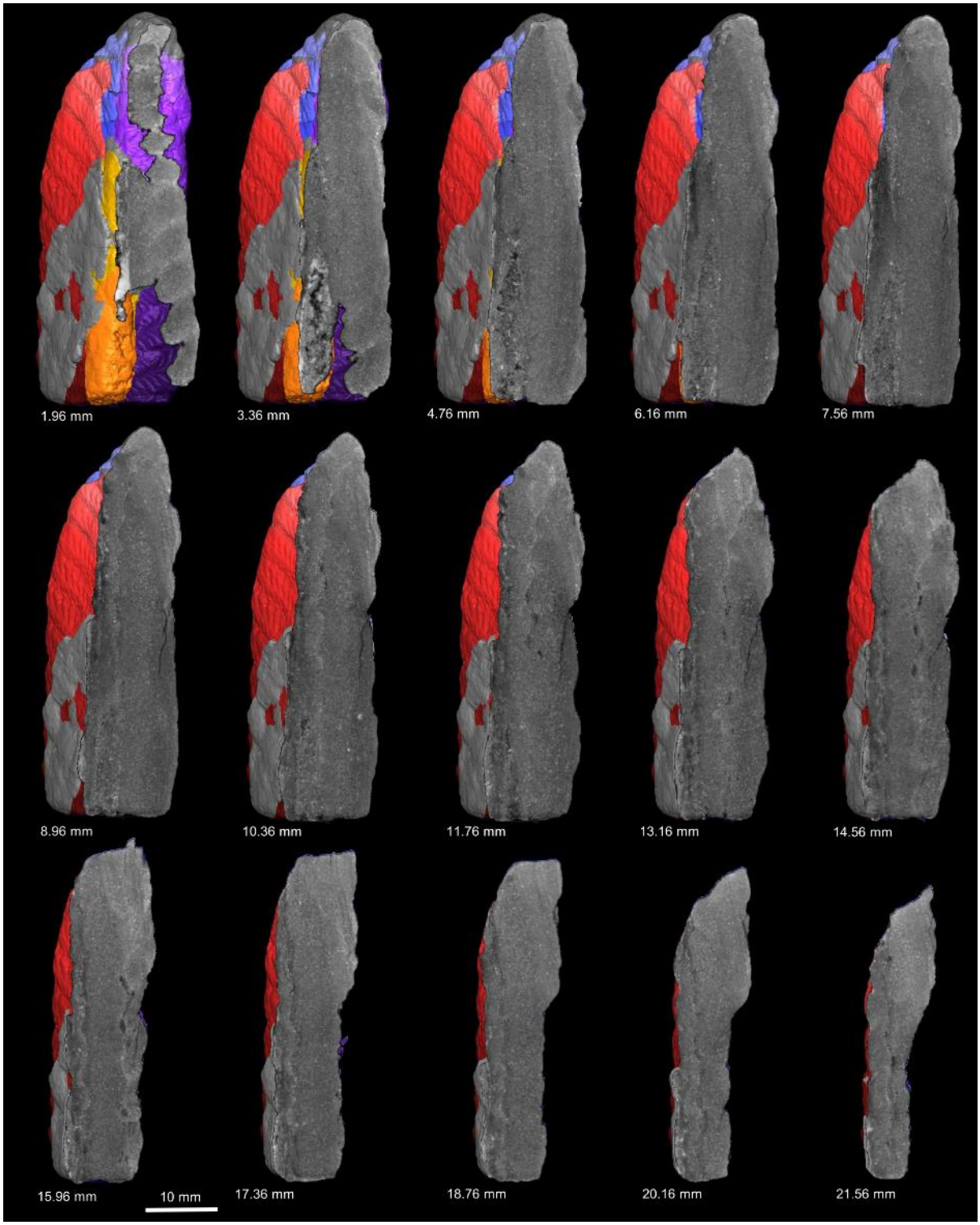

459

460 **Fig. S4.** CT sections though *Rangea* NESMF649 in the second longitudinal axis. The location
461 of each section (numbered) is 1.40 mm from the previous section in the series.

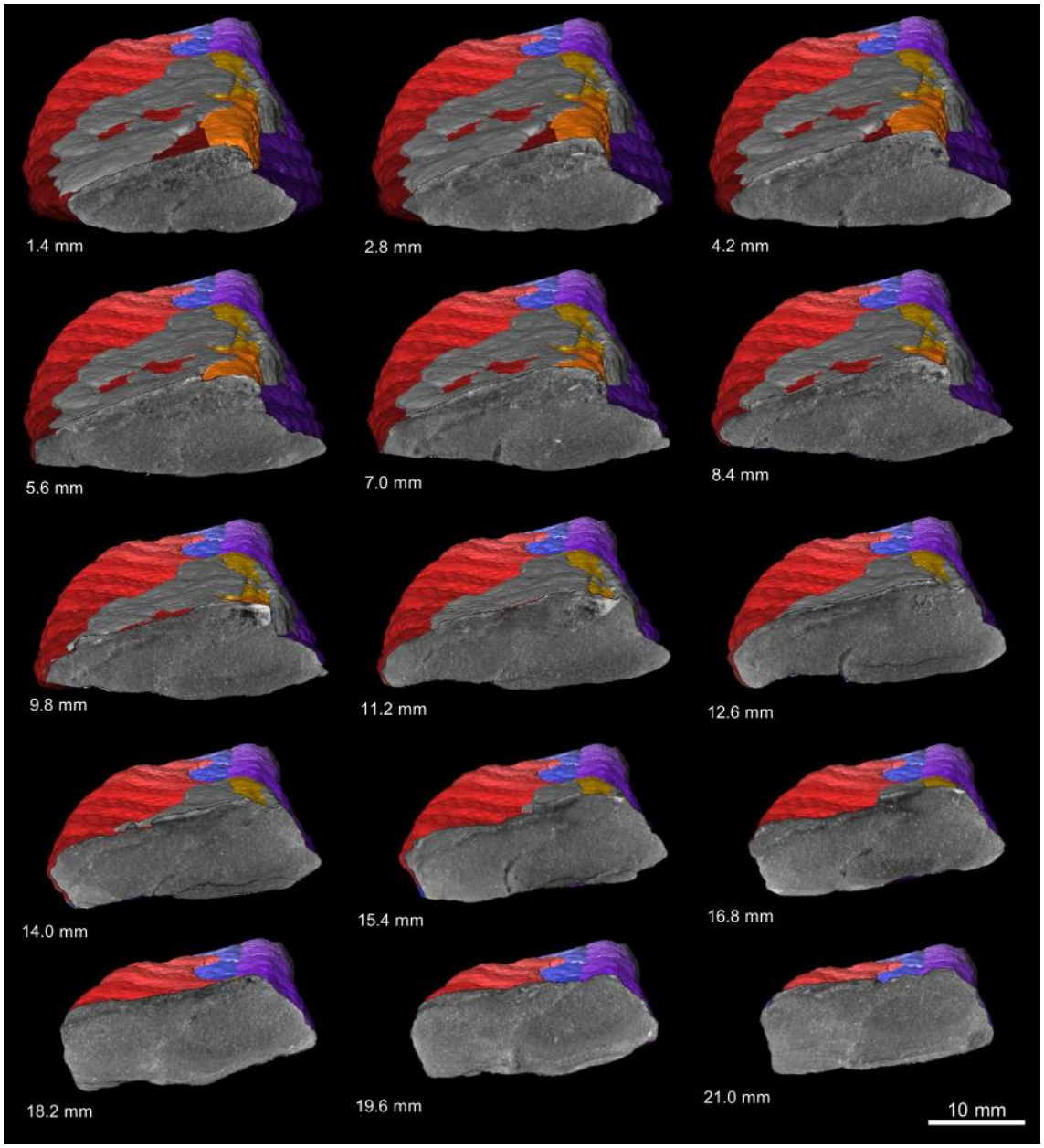

462

463 **Fig. S5.** CT cross sections though *Rangea* NESMF649. The location of each section
464 (numbered) is 1.40 mm from the previous section in the series.